Separation Science and Technology
Publication details, including instructions for authors and subscription information:
http://www.informaworld.com/smpp/title~content=t713708471

Obtainment of High-Fructose Solutions from Cashew (*Anacardium occidentale*) Apple Juice by Simulated Moving-Bed Chromatography

Diana C. S. Azevedo[a]; Alírio Rodrigues[b]
[a] GPSA, Department of Chemical Engineering, Federal University of Ceará, Brazil [b] LABORATORY OF SEPARATION AND REACTION ENGINEERING (LSRE), UNIVERSITY OF PORTO, PORTO, PORTUGAL

Online publication date: 19 December 2000

To cite this Article Azevedo, Diana C. S. and Rodrigues, Alírio(2000) 'Obtainment of High-Fructose Solutions from Cashew (*Anacardium occidentale*) Apple Juice by Simulated Moving-Bed Chromatography', Separation Science and Technology, 35: 16, 2561 — 2581
To link to this Article: DOI: 10.1081/SS-100102356
URL: http://dx.doi.org/10.1081/SS-100102356

SEPARATION SCIENCE AND TECHNOLOGY, **35**(16), pp. 2561–2581, 2000

Obtainment of High-Fructose Solutions from Cashew (*Anacardium occidentale*) Apple Juice by Simulated Moving-Bed Chromatography

DIANA C. S. AZEVEDO[†] and ALÍRIO RODRIGUES*
LABORATORY OF SEPARATION AND REACTION ENGINEERING (LSRE)
UNIVERSITY OF PORTO
FEUP—RUA DOS BRAGAS
4050-123 PORTO, PORTUGAL

ABSTRACT

The simulated moving-bed (SMB) technology has been successfully used in separations in the petrochemical, food, and fine chemicals industries. This work is intended to demonstrate the possibility of using this technology to obtain high-fructose solutions from the cashew apple juice, which may represent an attractive economic alternative for its industrial exploitation. The cashew tree is a native tropical plant abundant in Northeastern Brazil, the commercial value of which relies mainly on the processing of its nut. Despite the high nutritional value of the penduncle of the fruit, the cashew apple, approximately 90% of the crop spoils on the soil. Simulation and experimental results are presented for SMB separation of fructose from glucose, both present (~40 kg/m^3) in the aqueous phase of concentrated cashew apple juice. Kinetic and equilibrium data for fructose and glucose on packed columns using cation-exchange resins are reported. Experimental results for SMB operation at 30°C indicate purities close to 90% in each product (fructose-rich extract and glucose-rich raffinate). Simulated predictions of the unit performance and internal profiles agree well with experimental data. To increase the added value and versatility of the products, either an isomerization step for the raffinate or diverse SMB fluid–solid flow rate ratios may be applied. In this way, a wide range of products may be obtained, from nearly pure fructose to 42, 55, and 90% solutions, which are the standard high-fructose syrup concentrations. If solids content is conveniently raised to the standards of commercial high-fructose syrups, these products may be used as food additives, thus confirming a potentially attractive use of the cashew apple juice.

Key Words. Cashew juice; Fructose; Simulated moving bed

[†] GPSA, Department of Chemical Engineering, Federal University of Ceará, Brazil (on leave for Ph.D. training).
* To whom correspondence should be addressed. E-mail: arodrig@fe.up.pt

INTRODUCTION

The cashew tree (*Anacardium occidentale L.*) is a Brazilian tropical native plant that is cultivated in fields on the north coast of the country (the state of Ceará is its major producer) (1). The other two major world producers are Mozambique and India. The cashew agroindustry has an outstanding role in the economic and social context of these areas because it is a highly labor-intensive activity which offers one of the few, if not only, job opportunities in such underdeveloped areas. At present, according to Leite (2), the cashew nut is the most largely exported agro-product in the state of Ceará. Botanically speaking, the fruit of the tree is the nut, which is topped by a fleshy and juicy penduncle (see Fig. 1), whose color varies from yellow to intense red. This penduncle, also called the pseudofruit, apple, or pear, may be consumed "in natura" or it may be processed industrially to produce a wide range of products from concentrated juice to sweets. The local market basically consumes these industrially processed products and such industry does not play an important role in the economy of the state. Furthermore, sadly enough, the majority of the cashew apples produced spoil in the soil. In the state of Ceará, for instance, according to Price et al. (3), less than 10% of the annual production of cashew apples in 1974 was estimated to have been exploited industrially. This scenario seems not to have changed since 1974. A more recent record is given by Lopes Neto (4), who reports that the industrial exploitation of the cashew apple ranges from 2 to 6%. In such context, the use of the cashew apple as a source of high-added-value sugars may represent an attractive economic alternative for the Northeast region of Brazil. This work investigates the technical feasibility of obtaining high-fructose solutions from cashew apple juice using simulated moving-bed (SMB) technology, in a method similar

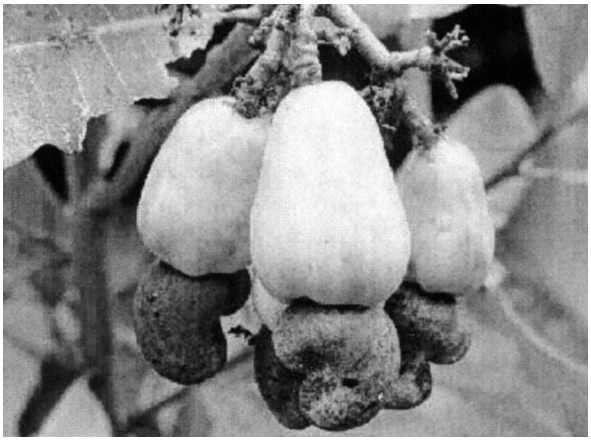

FIG. 1 Cashew apples and nuts.

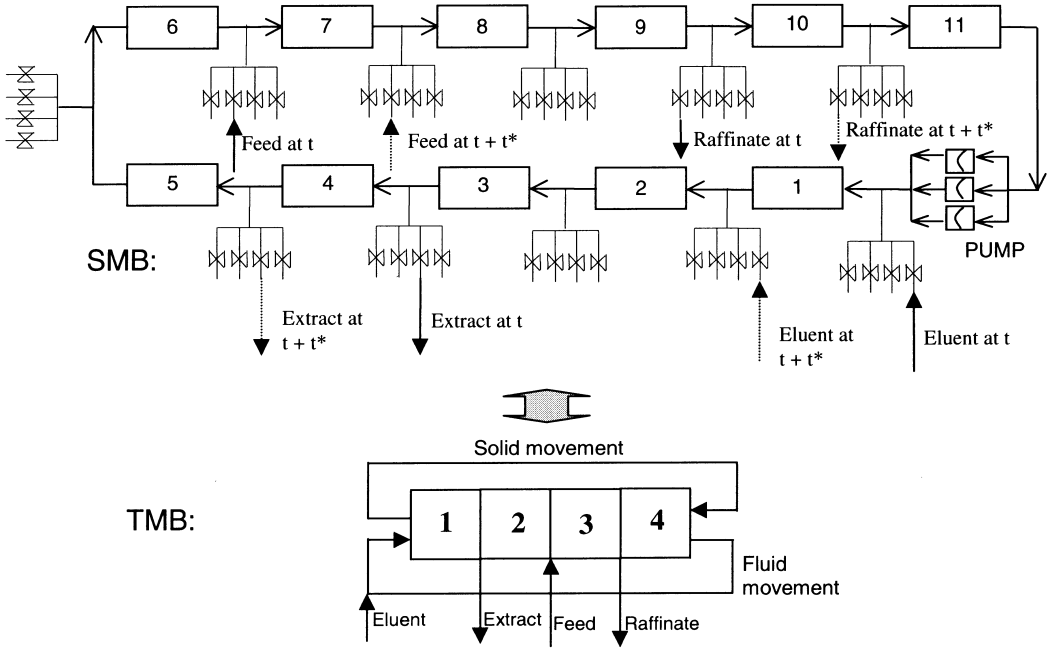

FIG. 2 Representation of the approaches of a real simulated moving-bed (SMB) and the equivalent true moving-bed (TMB) chromatography.

to that used to produce industrial high-fructose corn syrup (HFCS) widely used in the beverage and food industry.

The SMB technology has been successfully used for decades in separations that are difficult or highly energy consuming by conventional methods (e.g., distillation and crystallization). SMB is a chromatography-based technique, which consists of simulating the countercurrent motion of a solid adsorbent relative to a mobile phase. This is accomplished by having a set of fixed beds looped in a closed circuit with two inlet streams (feed and eluent/desorbent) and two outlet streams (extract and raffinate) and shifting their positions one bed ahead in the direction of fluid flow at regular time intervals (see Fig. 2).

The SMB technology is already industrially applied to the separation of fructose from glucose in a process known as SAREX based on the SORBEX technology as proposed by Universal Oil Products (UOP) (5). The separation of fructose from glucose by SMB chromatography is reported in the literature for different adsorbers, ion-exchange resins (6), and Y zeolite (7). To increase fructose purity and yield, application of temperature profiles has been proposed (8), as well as the combination of isomerization reactors with adsorption columns within the system (9, 10). Most recently, SMB has been proposed for sugar separation from biomass hydrolyzates (11, 12).

In SMB industrial fructose–glucose separation, the feed usually comes from the hydrolyzation of cornstarch and subsequent isomerization of glu-

cose. For the cashew apple juice, glucose and fructose are already present in equal amounts, which makes it an attractive raw material to be fed into an SMB plant. Some aspects yet to be considered are (a) the concentration of the feed, which may be as low as 4 g/100 g for each of the isomers for the juice "in natura"; and (b) the effects of other substances present (organic acids, mineral salts, and vitamins) on SMB operation. Furthermore, the insoluble pulp of the juice and the fruit wastes from the juice extraction process may the hydrolyzed to produce sugars of commercial interest. These aspects are out of the scope of this work and should be dealt with in forthcoming publications.

The present work shows chemical characterization data for cashew apple juice. Fructose and glucose were found to be the major constituents of the aqueous phase of cashew apple juice. Therefore, synthetic glucose–fructose mixtures, prepared to reproduce the composition of cashew apple juice, were used in SMB experiments in order to obtain high-fructose solutions. The results indicate an attractive use for this presently underestimated natural resource.

MATERIALS AND METHOD

Sugar Content Determination in Cashew Apple Juice

The cashew apple juice has been reported in the literature (1, 13) to be rich in carbohydrates, minerals, and vitamin C. The extracted juice is usually obtained through squeezing and sieving processes. It is composed of two phases: a solid phase, which is usually yellow and contains polysaccharides, insoluble pigments, and tannins, and an aqueous colorless phase, which is rich in carbohydrates and may be somewhat turbid due to tannins in suspension.

The sugar content of the aqueous phase of the juice was determined by HPLC analysis. Because of the difficulty in obtaining fresh fruit, two well-known brands of commercial cashew apple juice were analyzed. They are referred to as samples A and B. Samples of the supernatant liquid which topped the solid phase inside the bottles were collected and centrifuged (5000 rpm) until a clear supernatant was obtained. These clarified samples were diluted (1:1) and injected in a chromatographic ion-exchange column connected to a refractive index detector. The obtained chromatograms were compared with other chromatograms of the following standards: ascorbic acid, citric acid, fructose, glucose, and sucrose. These substances are reportedly present in the aqueous phase of cashew apple juice.

Column Packing and Characterization

Eleven Superformance® glass columns SP 300 × 26 (Götec Labortechnik, Mühltal, Germany), to be used in the SMB pilot plant, were packed with the gel-type, cation-exchange resin Dowex Monosphere 99/Ca (Supelco, Belle-

fonte, PA) by the slurry method. These columns have a thermostatic jacket for temperature control, 2.6 cm internal diameter, and an adjustable length of 25–30 cm. They were packed 29 cm long each and subjected to a flow rate of 30 mL/min. A 30-bar back pressure was maintained by placing a valve at the exit of each column for 30 min to ensure complete settling of the packing and eliminate any dead volume. The following determinations were carried out to estimate required parameters for the SMB model:

1. Tracer pulse experiments were conducted using a blue dextran solution (5 g/L). Samples of 0.2 mL were injected under different flow rates and the column response was monitored using a UV detector. The bed porosity was calculated from the stoichiometric time of the obtained experimental curves. By calculating the second moment of the experimental curve, an average Peclet number was obtained for the range of flow rates to be employed in the SMB (25–40 mL/min). The same procedure was used with sucrose solutions in order to calculate particle porosity.
2. Equilibrium isotherm determination for fructose and glucose onto the cationic resin was conducted by the column saturation method, which consisted of the following steps: (*a*) A solution of fructose–glucose of known composition (C_0) was pumped through the column for enough time to ensure complete saturation of the adsorbent. This may be done by monitoring the outlet concentration with an RI detector. (*b*) Fresh eluent (deionized water) was then pumped through the previously saturated column for as much time as in the saturation step (linear isotherms assumed). The eluate must be collected in a previously weighed reservoir. (*c*) The concentration of the eluate (C_{el}) was measured for both fructose and glucose. (*d*) When the initial solution concentration (C_0), the volume of eluate (V_{el}), the bed void fraction (ε), the bed volume (V_{col}), any extra-column volume (V_{ex}), and the concentration of the eluate (C_{el}) were known, the adsorbed phase concentration (q_{ads}) in equilibrium with C_0 was given by the following equation:

$$q_{ads} = \frac{V_{el}C_{el} - C_0\,(\varepsilon V_{col} + V_{ex})}{(1-\varepsilon)V_{col}} \tag{1}$$

   (*e*) The procedure described in items (*a*) through (*d*) was repeated for another fluid phase concentration C_0.
3. Pulse, breakthrough, and elution experiments were conducted with fructose and glucose individual solutions. By comparison with the corresponding simulated curves and through a "best-fit" procedure, equilibrium and kinetic data for both fructose and glucose were calculated.
4. A pulse experiment with a glucose–fructose binary solution was conducted using the whole set of SMB columns placed in series.

TABLE 1
Experimental Conditions Used in SMB Experiment

Model parameters	Operating conditions	Columns
Pe = 1500	$T = 30°C$	$D_b = 2.6$ cm
$Bi_m = 500$	Feed concentration, $C_F = 40$ g/L each	$L_b = 29$ cm
		Configuration: 3-3-3-2
$k_p = 2\ min^{-1}$	$t^* = 3.4$ min	$\gamma_1 = 1.1$
		$\gamma_2 = 0.51$
$k_\mu = 0.8\ min^{-1}$	$Q_{Rec} = Q_4 = 24$ mL/min	$\gamma_3 = 0.66$
		$\gamma_4 = 0.32$
$K_{FR} = 0.5 \quad K_{GL} = 0.18$	$Q_{EL} = 14.04$ mL/min	
$\varepsilon_p = 0.1$	$Q_X = 10.7$ mL/min	
	$Q_F = 2.72$ mL/min	
	$Q_R = 6.06$ mL/min	

SMB Experiments

The 11 SP 300 × 26 columns were connected to the SMB pilot plant, LICOSEP® 12–26 (Novasep, Champignelles, France). The jackets were connected to one another by silicone hoses and to a thermostated bath (Lauda, Lauda-Königshofen, Germany). Between every two columns there was a four-port valve actuated by the control system. When required, the valves allowed either pumping of feed/eluent into the system or withdrawal of extract/raffinate streams so as to execute the switching scheme described in the Introduction section. Each of the inlet (feed and eluent) and outlet (extract and raffinate) streams was pumped by means of Merck–Hitachi (Darmstadt, Germany) HPLC pumps.

SMB experiments were conducted for glucose–fructose separation by pumping the binary solution as feed and using distilled deionized water as eluent. The operating conditions are those shown in Table 1. The dispersion, kinetic, and equilibrium parameters shown in the first column of the table were those measured from the experiments described in the previous section. The operating conditions were chosen from a design procedure as described in previous work (14).

MATHEMATICAL MODELING

SMB Model

The theoretical model chosen to represent an SMB was that of a true countercurrent or true moving bed (TMB). Figure 2 shows the difference between the concepts of an SMB and a TMB. In the TMB representation, the solid

moves countercurrently in relation to the fluid phase and the problem is reduced to writing the pertinent mass balance equations for each of the species involved in each of the four countercurrent sections, together with the global mass balances in the eluent, feed, raffinate, and extract nodes. The mathematical model proposed to represent the steady state of species *i* in a section *j* of a true countercurrent unit is presented in equations (2) to (17). Axially dispersed flow is assumed for the fluid phase and plug flow is assumed for the solid phase. Diffusion through the external film is also considered and intraparticle mass transfer is described by means of a bilinear driving force approximation described elsewhere (15).

- Mass balance in outer fluid phase:

$$\frac{1}{\mathrm{Pe_j}}\frac{d^2C_{ij}}{dx^2}-\frac{dC_{ij}}{dx}-\frac{(1-\varepsilon)}{\varepsilon}\left[\frac{\mathrm{Bi}_{mj}}{5+\mathrm{Bi}_{mj}}\,\alpha_{\mathrm{p}ij}\,(C_{ij}-\bar{C}_{\mathrm{p}ij})\right]=0 \qquad (2)$$

- Mass balance in intraparticle fluid phase (pores):

$$\frac{1}{\gamma_j}\frac{d\bar{C}_{pij}}{dx}+\frac{\mathrm{Bi}_{mj}}{5+\mathrm{Bi}_{mj}}\frac{\alpha_{pij}}{\varepsilon_{\mathrm{p}}}\,(C_{ij}-\bar{C}_{\mathrm{p}ij})-\frac{\alpha_{\mu_{ij}}}{\varepsilon_{\mathrm{p}}}\,\rho_{\mathrm{p}}\left[\frac{K_i}{\rho_{\mathrm{p}}}\,\bar{C}_{\mathrm{p}ij}-\langle\bar{q}\rangle_{ij}\right]=0 \qquad (3)$$

- Mass balance in intraparticle "solid" phase (microparticles):

$$\frac{1}{\gamma_j}\frac{d\,\langle\bar{q}\rangle_{\mathrm{ij}}}{dx}+\alpha_{\mu_{ij}}\left[\frac{K_i}{\rho_{\mathrm{p}}}\,\bar{C}_{\mathrm{p}ij}-\langle\bar{q}\rangle_{ij}\right]=0 \qquad (4)$$

- Boundary conditions for section *j*:

At $x = 0$:

$$C_{ij}^{\mathrm{in}}=C_{ij}\,(0)-\frac{1}{\mathrm{Pe}_j}\frac{dC_{ij}}{dx} \qquad (5)$$

At $x = 1$:

$$\frac{dC_{ij}}{dx}\,(1)=0 \qquad (6)$$

$$\bar{C}_{\mathrm{p}ij}\,(1)=\bar{C}_{\mathrm{p}i(j+1)}\,(0) \qquad (7)$$

$$\langle\bar{q}\rangle_{ij}\,(1)=\langle\bar{q}\rangle_{i(j+1)}\,(0) \qquad (8)$$

The space dimensionless variable is $x = z/L_j$, where L_j is the length of *j*th section. The dimensionless numbers present in the model equations are

- Fluid-solid flowrate ratio:

$$\gamma_j=\frac{U_{\mathrm{F}j}}{U_{\mathrm{s}}} \qquad (9)$$

- Number of macropore mass transfer units:

$$\alpha_{\mathrm{p}ij} = \frac{k_{\mathrm{p}i} L_j}{U_{\mathrm{F}j}} \tag{10}$$

- Number of microparticle mass transfer units:

$$\alpha_{\mu_{ij}} = \frac{k_{\mu_i} L_j}{U_{\mathrm{F}j}} \tag{11}$$

- Mass Biot number (film diffusion/effective pore diffusion):

$$\mathrm{Bi}_{mj} = \frac{k_{fj} R_{\mathrm{p}}}{D_{\mathrm{pe}}} \tag{12}$$

- Peclet number (convection/dispersion):

$$\mathrm{Pe}_j = \frac{U_{\mathrm{F}j} L_j}{D_{ax}} \tag{13}$$

C^{in} present in the boundary condition at the section inlet can be found from the node balances.

- Eluent node:

$$C_{i1}^{\mathrm{in}} = \frac{Q_4}{Q_4 + Q_{\mathrm{E}}} C_{i4}\,(1) \tag{14}$$

- Extract node:

$$C_{i2}^{\mathrm{in}} = C_{i1}\,(1) \tag{15}$$

- Feed node:

$$C_{i3}^{\mathrm{in}} = \frac{Q_2}{Q_3} C_{i2}\,(1) + \frac{Q_{\mathrm{F}}}{Q_3} C_{i\mathrm{F}} \tag{16}$$

- Raffinate node:

$$C_{i4}^{\mathrm{in}} = C_{i3}\,(1) \tag{17}$$

In this approach, the steady-state concentrations are constant for both of the products (extract and raffinate) and the concentration profile throughout the column is fixed. On the other hand, a real SMB reaches the steady state in a periodic fashion. The internal concentration profiles move along the axial direction in a periodic way. Therefore, the product (extract and raffinate) concentrations vary within a period, even though the cycle average is the same as that calculated from the TMB model at steady state. The average concentration at a given point measured over a rotation period should be equal to the

concentration calculated from a TMB model at that point. For comparison of modeling results with experimental data, the internal SMB profile is sampled and measured at 50% of a period. This equivalence between models has been shown before (16) for as few as two columns per section. Because we used three columns per section (except in section 4) and the TMB model requires a much less computational effort, this approach was chosen to predict SMB performance.

The system of 24 (4 sections $\times$ 2 components $\times$ 3 equations) ordinary differential equations was solved by using the package COLNEW (17). Spatial discretization was performed by modified B-splines assuming 14 finite elements per section with two collocation points in each element. The integrator tolerance was set at 10^{-9}. A maximum tolerance of 1% was defined for the sum of errors from global mass balance (amount that leaves – amount that enters) and product concentration at each consecutive iteration. Model solutions were obtained after an average of 20 iterations, and run times were typically 10 sec on a Pentium II 300 MHz processor.

The key to a correct design of an SMB unit relies on the correct choice of flow rate ratios, γ_j. There are constraints on these flow rates which must be observed, especially on sections 2 and 3, where adsorption occurs. In the simplest case, if dispersion and mass transfer effects are neglected, Ruthven and Ching (18) have shown the effect of the relative values of γ_2 and γ_3 on the quality of separation. They are summarized as follows:

If	$\nu K'_B < \gamma_2 < \gamma_3 < \nu K'_A$	pure extract and raffinate are obtained
If	$\gamma_2 < \nu K'_B$ and $\nu K'_B < \gamma_3 < \nu K'_A$	only pure raffinate is obtained
If	$\gamma_3 > \nu K'_A$ and $\nu K'_B < \gamma_2 < \nu K'_A$	only pure extract is obtained
If	$\gamma_2 < \nu K'_B$ and $\gamma_3 > \nu K'_A$	no separation is obtained

where ν is the solid/fluid phase ratio, $(1 - \varepsilon)/\varepsilon$, and $K' = K + \varepsilon_p$. A represents the preferentially adsorbed component and B represents the weakly adsorbed component. However, when mass transfer resistances are present, the regions of separation move and are no longer delimited by straight lines, which are only dependent on equilibrium data. Figure 3 qualitatively shows this effect. As mass transfer effects become significant, which is the general case in ion exchange resins, the region of separation "shrinks" and may eventually disappear if very high purities are pursued. The term "separation" refers to high purities in both extract and raffinate. Such "high purity" may be as low as 90%, for instance, and must be defined prior to plant operation so that the corresponding region of separation for that desired purity may be accessed through simulation. Details of this design methodology which take mass transfer effects into consideration may be found in previous work (14).

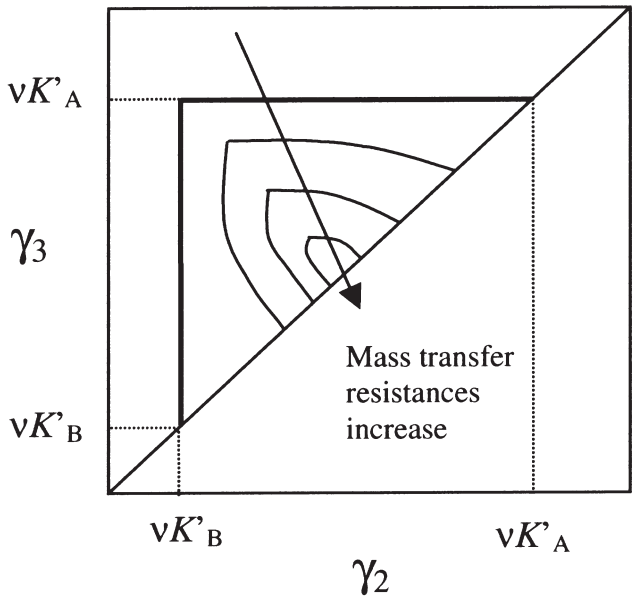

FIG. 3 Regions of complete separation for linear isotherm systems based on the equilibrium model and with mass transfer resistances considered.

Isomerization Reactor Model

The glucose-rich raffinate stream may be isomerized by the glucose–isomerase enzyme according to the reversible reaction shown below:

$$\text{Glucose} \underset{k_r}{\overset{k_{-r}}{\rightleftharpoons}} \text{Fructose}$$

A 42% fructose solution may be obtained, which is a commercial standard for fructose syrups. This is usually done in a fixed bed with the immobilized enzyme. A simple transient model, as proposed by Ching and Lu (10), was used. It considers only axial dispersion for the fluid phase and pseudo-first-order reaction kinetics.

For a component i (for fructose i = A, and for glucose i = B):

$$\frac{\partial C_i}{\partial \theta} = \frac{1}{\text{Pe}} \frac{\partial^2 C_i}{\partial x^2} - \frac{\partial C_i}{\partial x} - \frac{(1-\varepsilon)}{\varepsilon} r_i \tag{18}$$

where

$$-r_A = r_B = \text{Da}(K_r^{eq} C_B - C_A) \tag{19}$$

The dimensionless variables are $x = z/L_b$ and $\theta = tU_F/L_b$. The parameter Da is the reaction Damkohler number, defined as $k_r L_b/U_F$. According to Camacho-Rubio et al. (19), for the immobilized enzyme Sweetzyme T® (Novo, Bagsvaerd, Denmark), the following correlations apply for the reaction equi-

librium and kinetic parameters at 323 K:

$$K_r^{eq} = 24.3 \exp(-1022/T) \quad (20)$$

$$k_r = 7.7 \times 10^3 \rho_b \exp(-6300/T) \quad (21)$$

The boundary and initial conditions are

$$\text{At } x = 0 \qquad C_i^{in} = C_i(0,\theta) - \frac{1}{Pe}\frac{\partial C_i}{\partial x} \quad (22)$$

$$\text{At } x = 1 \qquad \frac{\partial C_i}{\partial x}(1,\theta) = 0 \quad (23)$$

$$\text{At } \theta = 0 \qquad C_i(x,0) = 0 \quad (24)$$

RESULTS

Cashew Apple Juice Characterization

Samples of cashew apple juice from two commercial brands were analyzed by HPLC for sugar content assessment. The aqueous colorless phase was collected and centrifuged. The supernatant was diluted in equal volume of pure water and injected into a chromatographic column connected to a refractive index detector. The analysis parameters were mobile phase, 0.005 N H_2SO_4 solution; mobile phase flow rate, 0.3 mL/min; pressure, 90 bar; column, organic acids column Interaction ION-300, 300 × 7.8 mm; and sample volume, 20 μL.

Figure 4 shows chromatograms of samples of the two brands of cashew apple juice labeled as A and B. Good reproducibility between the two commercial brands was observed. A significant amount of ascorbic acid was verified, confirming long-term literature records (20) about the nutritious value of the fruit. However, the amount of vitamin C was nearly one-third of that measured for the fresh fruit (1) due to oxidation caused by light and oxygen.

These chromatograms were compared with chromatograms (not shown) of standard solutions of glucose, fructose, sucrose, citric acid, and ascorbic acid, obtained under the same analysis conditions. Comparison with cashew apple juice composition as given by other authors allowed us to propose the identification of the peaks as presented in Table 2. Peaks 1, 2, and 8 could not be identified and may be pigments, polysaccharides, or tannins. The average sugar content found in both samples of juice is around 40 g/L for each of the sugars (glucose and fructose), or 4 g/100 g juice. This figure is in accordance with literature records (1, 13), which mention a sugar content of 4–11.9 g/100 g present in the aqueous phase of cashew apple juice.

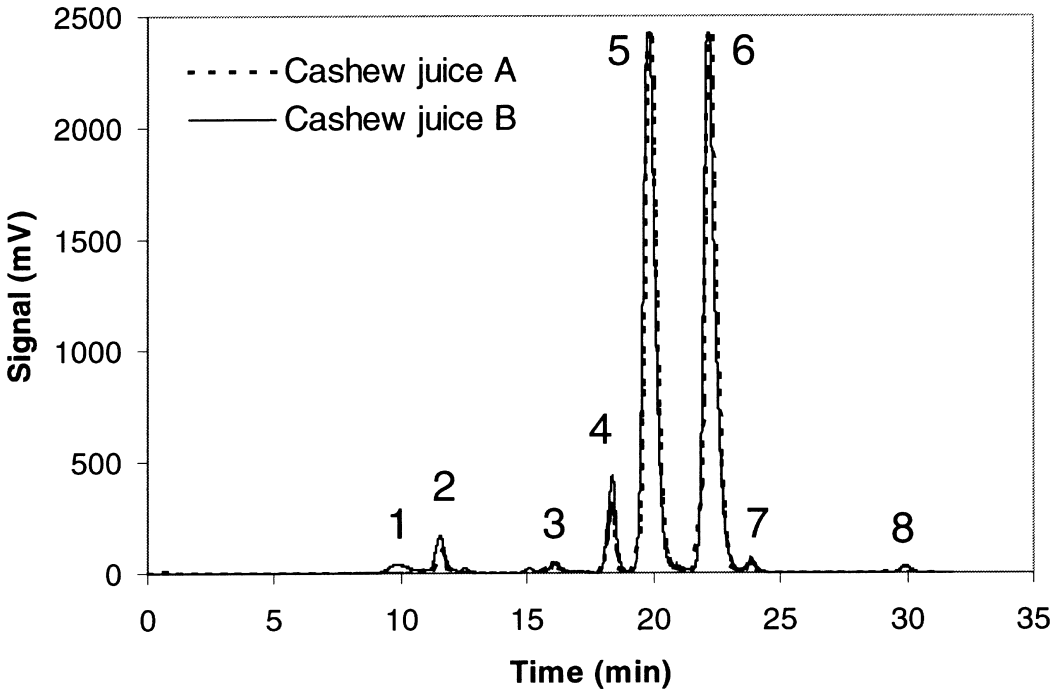

FIG. 4 Chromatograms of two brands of commercial concentrated cashew apple juice and standards of commercial vitamin C, fructose, glucose, and sucrose.

Estimation of Model Parameters

From pulse experiments in each of the 11 SMB columns using blue dextran as a tracer, it was possible to determine the bed porosity and Peclet number from the obtained response curves. The calculated average values were 0.4 for

TABLE 2
Composition of Clarified Cashew Apple Juice

			Cashew juice A		Cashew juice B	
Peak	Component	Reported concentration (g/100 g)[a]	Retention time (sec)	Concentration (g/100 g)	Retention time (sec)	Concentration (g/100 g)
1	(Unknown)	–	–	–	597	–
2	(Unknown)	–	694	–	694	–
3	Sucrose	0.08	967	0.051	964	0.042
4	Citric acid	0.224–0.828	1100	0.64	1102	0.42
5	Glucose	4.0–11.9	1208	3.99	1212	3.92
6	Fructose	(glucose + fructose)	1345	3.85	1344	3.90
7	Ascorbic acid	0.121–0.231	1430	0.052	1430	0.056
8	(Unknown)	–	–	–	1795	–

[a] Source: reference 1.

the bed porosity and 500 for the Peclet number. The particle porosity was calculated using this very same experimental procedure for sucrose solutions. The characteristic stoichiometric time is proportional to the total porosity $\varepsilon + (1 - \varepsilon)\varepsilon_p$. Because ε was found to be 0.4, particle porosity given by this experiment was 0.1.

The isotherms were measured in the range of 0–30 g/L at 30°C according to the column saturation method as described previously. The isotherms, illustrated in Fig. 5, are linear in this concentration range with equilibrium constants equal to 0.29 and 0.55 for glucose and fructose, respectively, assuming the adsorbent to be a homogeneous solid.

The pulse curves obtained for pure fructose and glucose solutions (not shown) were well correlated by simulation with $K'_{GL} = 0.24$, $K'_{FR} = 0.58$, $k_p = 2\ min^{-1}$, and $k_\mu = 0.8\ min^{-1}$. As for the breakthrough and elution experiments, Fig. 6 shows the curves obtained for pure fructose and glucose solutions. In each graph the equilibrium constant calculated from the experimental stoichiometric time is shown. These calculated values were used in the simulation of the curves. For all simulations, $k_p = 2\ min^{-1}$ and $k_\mu = 0.8\ min^{-1}$ (for both isomers) resulted in a best fit of the experimental data.

Table 3 summarizes the model parameters obtained for the various experiments described at 30°C. The average values shown in the last row were those used in the simulation of the SMB performance. They are included in Table 1 as the experimental conditions in which the SMB pilot plant was operated.

To obtain a final confirmation of the dispersion, equilibrium, and kinetic parameters obtained through the previously described experiments, a pulse experiment was conducted in the 11 SMB columns placed in series using a binary glucose and fructose solution. A sample of 300 mL and 20 g/L was injected into the set of 11 columns and then eluted under a flow rate of 30

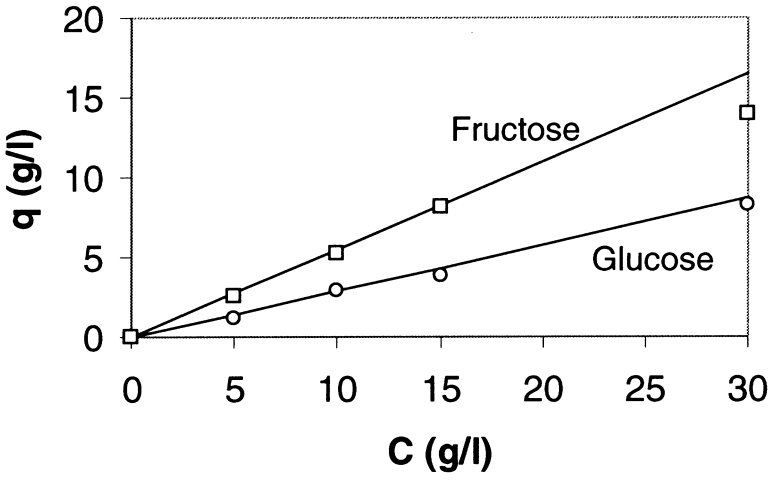

FIG. 5 Fructose and glucose isotherms on Dowex Monosphere 99/Ca at 30°C.

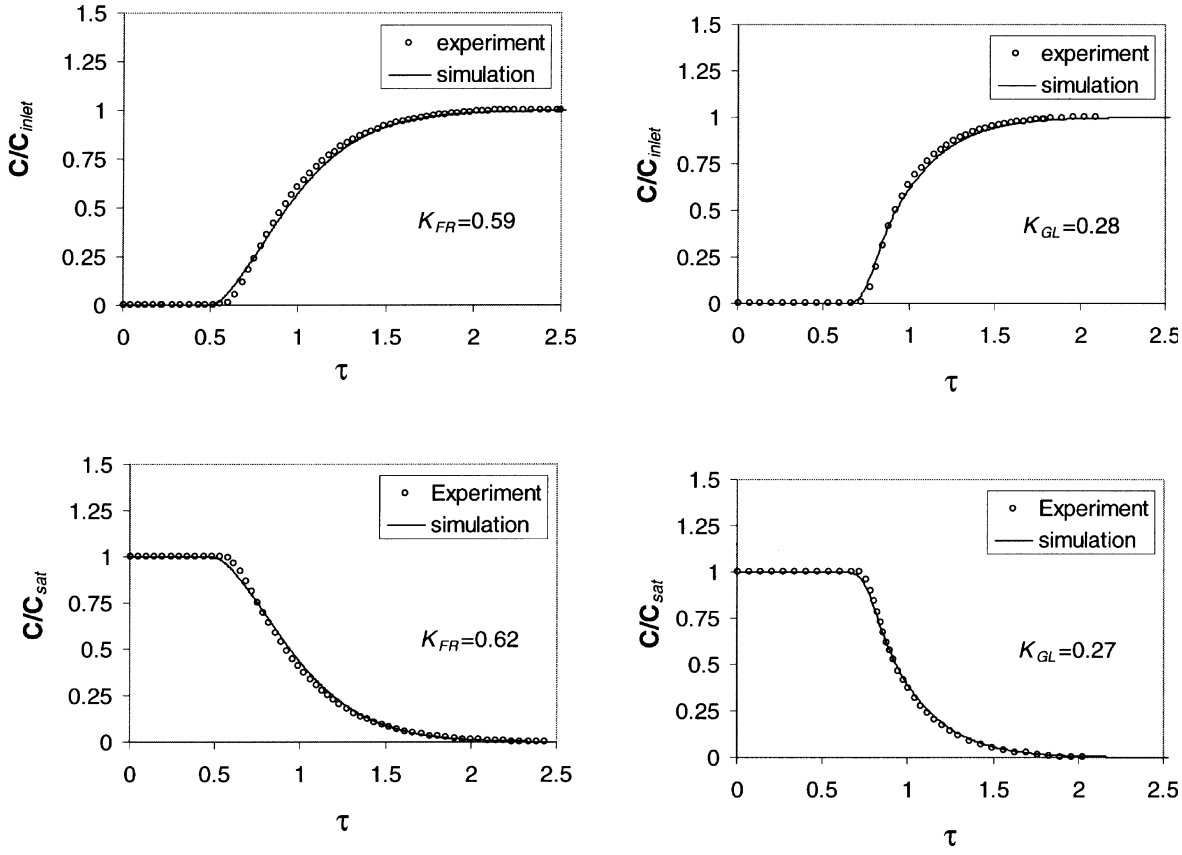

FIG. 6 Fructose and glucose breakthrough and elution curves on a fixed bed packed with cation-exchange resin Dowex Monosphere.

TABLE 3
Summary of the Estimated Parameters from Various Experiments

	Estimated parameter						
Experiments of type	Pe	ε	ε_p	K'_{FRU}	K'_{GLU}	k_p, min^{-1}	k_μ, min^{-1}
A	500	0.4	–	–	–	–	–
B	–	–	–	0.55	0.29	–	–
C	500[a]	0.4[a]	0.1[a]	0.58[b]	0.24[b]	2	0.8
D	500[a]	0.4[a]	0.1[a]	0.59[b]	0.28[b]	2	0.8
E	500[a]	0.4[a]	0.1[a]	0.62[b]	0.27[b]	2	0.8
Average	500	0.4	0.1	0.60	0.28	2	0.8

A: Column dispersion determination, tracer experiment with blue dextran.
B: Isotherm determination, dynamic method.
C: Pulse experiments with pure fructose and glucose.
D: BTC experiment with pure fructose and glucose.
E: Elution experiment with pure fructose and glucose.
[a] Input to the simulation of experimental data.
[b] Measured from the experimental curve stoichiometric time.

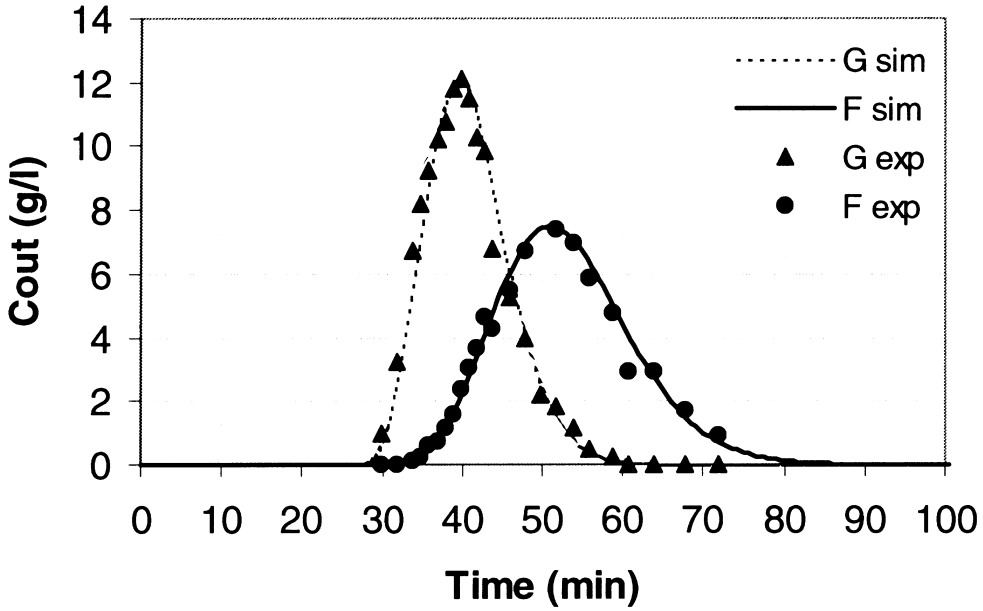

FIG. 7 Pulse experiment using the 11 SMB columns placed in series.

mL/min. Figure 7 shows the exit concentration obtained experimentally compared with the simulated curves. Very good agreement is obtained for $K'_{FR} = 0.6$, $K'_{GL} = 0.28$, $k_p = 2\ min^{-1}$, and $k_\mu = 0.8\ min^{-1}$.

SMB Experiments

The LICOSEP 12–26 unit was operated under the conditions shown in Table 1. These operating conditions were chosen following the procedure outlined below:

1. A safety margin of approximately 25% was applied to the constraints on γ_1 and γ_4 stated by the equilibrium theory (γ_1^{eq} and γ_4^{eq}), so that $\gamma_1 = 1.25 \times \gamma_1^{eq} = 1.1$ and $\gamma_4 = \gamma_4^{eq}/1.25 = 0.32$.
2. The minimum flow rate pumped with precision by the SMB recycling pump, 24 mL/min, was taken to be the flow rate in section 4.
3. The corresponding switching time, t^*, for $\gamma_4 = 0.32$ and $Q_4 = 24$ mL/min was found to be 3.4 min.
4. Having determined t^*, γ_1, and γ_4, values of γ_2 and γ_3 within the separation triangle defined by the equilibrium theory were successively chosen, the corresponding SMB operating conditions were calculated, and the process performance was simulated by using the model presented in this work.
5. The (γ_2; γ_3) values which result in purities of both products higher than 90% define a new "region of separation" with mass transfer resistances

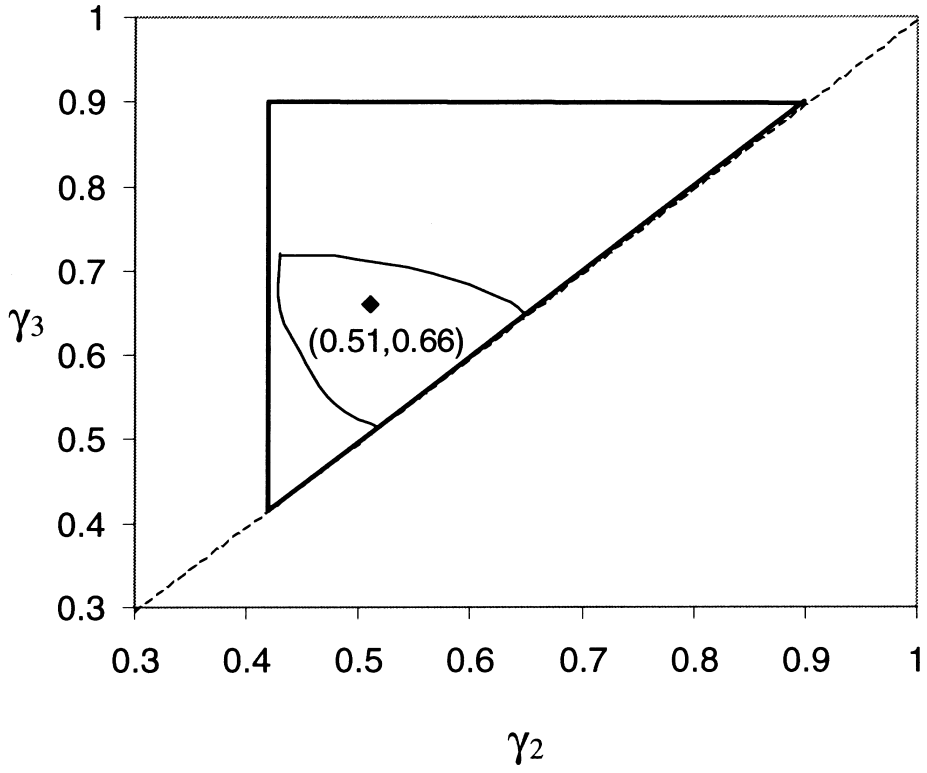

FIG. 8 Separation region (both product purities above 90%) for SMB pilot unit LICOSEP at 30°C. The point inside the region is the chosen SMB operating point.

taken into account. Figure 8 shows the "separation region" obtained following this procedure. The operating point (0.51; 0.66) was selected to define the operating conditions for an experiment. It is far enough from both limits, which ensures robust operation, and far enough from the diagonal ($Q_F = 0$), which means improved adsorbent productivity.

Steady-state attainment was monitored by collection of samples of extract and raffinate for a whole cycle at every 2 cycles and measuring the corresponding concentrations. When these concentrations remained unchanged and mass balances for both fructose and glucose were checked (amount that enters equals amount that leaves), the internal concentration profile was sampled and measured; this occurred in the 15th cycle. Figure 9 shows the experimental steady-state concentration profile compared with that obtained by simulation. Very good agreement between the predicted and the experimental profiles can be observed. For the extract sample collected for a whole cycle, 87% purity was obtained experimentally, 87.4% purity was obtained from a sample collected at 50% of a period during the same cycle, and 91.7% purity was predicted from numerical simulation. For the raffinate, these figures were 88.6,

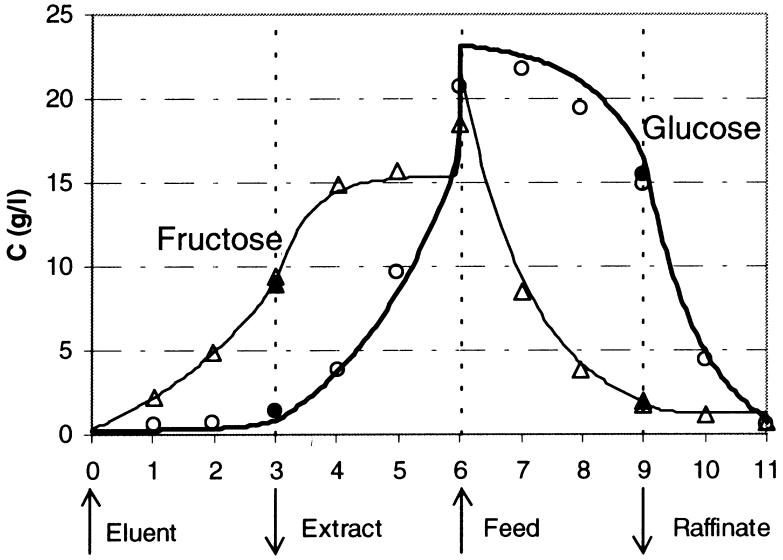

FIG. 9 SMB internal profile. Black points indicate cycle average concentrations.

89.2, and 89.4%, respectively. In all cases, experimental performance was worse than that predicted from simulation. This may be due to the use of the TMB model instead of the real SMB; the first approach usually resulted in more optimistic results, as shown by other authors (16). At higher sugar concentration, the isotherms may exhibit some degree of nonlinearity, which was not accounted for in our model.

Because our target product is fructose, one may obtain a higher fructose-enriched extract by increasing γ_2 and/or γ_3 values at the expense of decreasing the raffinate purity. For instance, if $\gamma_2 = 0.83$ and $\gamma_3 = 0.98$, and the other operating conditions are those shown in Table 4, a 97% fructose solution is obtained in the extract and a 42% fructose solution is obtained in the raffinate. Convenient mixing of these two streams in the right proportion may yield a 55% fructose solution. This may be desirable in order to obtain products at 42 and 55% fructose, which are standards for high-fructose syrups (21).

Alternatively, the raffinate stream obtained in the experiment illustrated in Table 1 may be isomerized with the immobilized enzyme glucose–isomerase in a fixed bed reactor. If the 89% raffinate stream obtained in the experiment described in Fig. 7 is fed into a fixed bed isomerization reactor under the conditions described in Table 5, it may be converted to a 42% fructose stream after 100 min. Again, convenient mixing of the reactor effluent and the extract stream may result in a 55% fructose solution.

Yet to be investigated is the concentration of the high-fructose solutions shown in this work compared to the commercial high-fructose syrups. The

TABLE 4
Operating Conditions for SMB in Order to Obtain a More Fructose-Enriched Extract

Model parameters	Operating conditions	Columns
Pe = 1500	T = 30°C	D_b = 2.6 cm
Bi_m = 500	Feed concentration, C_F = 40 g/L each	L_b = 29 cm
		Configuration: 3-3-3-2
$k_p = 2\ min^{-1}$	t^* = 3.4 min	γ_1 = 1.1
		γ_2 = 0.83
$k_\mu = 0.8\ min^{-1}$	$Q_{Rec} = Q_4$ = 23 mL/min	γ_3 = 0.98
		γ_4 = 0.27
K_{FR} = 0.5 K_{GL} = 0.18	Q_{EL} = 14.04 mL/min	
ε_p = 0.1	Q_X = 3.89 mL/min	
	Q_F = 2.72 mL/min	
	Q_R = 12.87 mL/min	

Expected performance (from numerical simulation)

Purity	Recovery
97% fructose solution in extract (8.4 g/l)	29% fed fructose is collected in extract
58% glucose solution in raffinate (14 g/l)	99% fed glucose is collected in raffinate

solids content in syrups should, by law, be no less than 70% wt (22) and the solutions obtained in this work have a solids content as low as 2% wt. The concentration process is usually carried out by nanofiltration or evaporation under vacuum. Because these are costly unit operations, their correct economic evaluation is fundamental to define the feasibility of the whole process. Another aspect to be considered is the effect of cashew apple juice trace components (mineral salts, organic acids, and tannins) on the resin and, hence, on the SMB performance. The insoluble matter present in the juice, which is basically composed of polysaccharides, may also be a source of fructose after con-

TABLE 5
Operating Conditions for an Isomerization Reactor

Model parameters	Operating conditions	Reactor dimensions
Pe = 500	T = 50°C	D_b = 2.6 cm
$k_r = 0.0617\ min^{-1}$	Feed concentration: 2 g/L fructose, 16 g/L glucose	L_b = 60 cm
ε = 0.4	Q_F = 2.72 mL/min	
K_r^{eq} = 1		

Reactor performance from numerical simulation

X_{eq} = 36% (glucose-based) reached after 100 min

venient chemical transformations such as acid hydrolysis. All of these subjects should be addressed in future work.

CONCLUSIONS

This work proposes a potential economically beneficial alternative for the cashew apple juice as a fructose source. HPLC analysis of the juice aqueous phase indicated significant presence of both fructose and glucose in equal amounts. A binary mixture of fructose and glucose was separated by SMB chromatography using operating conditions defined with the aid of the proposed mathematical model. Some interesting points highlighted by this work are (*a*) the experimental determination of mass transfer parameters for the recently proposed bi-linear driving force approach and the excellent agreement between the simulations carried out with such parameters and experimental SMB profiles; and (*b*) the achievement of a satisfactory separation despite the use of relatively small adsorbent inventory. Choice of different operating conditions and/or isomerization of the glucose-rich product may lead to a wide range of fructose syrups if solids content (Brix) is conveniently elevated to industrial standards. Further investigation on the effects of other cashew juice trace components and economic evaluation of complementary unit operations are necessary to confirm the feasibility of the cashew apple juice as a fructose resource.

NOMENCLATURE

C	outer-particle fluid phase concentration, kg/m^3
C^{in}	column/section inlet concentration, kg/m^3
C^{inlet}	column inlet concentration in breakthrough experiments (Fig. 6), kg/m^3
C_{el}	eluate concentration, kg/m^3
C_0	initial bulk fluid phase concentration (Eq. 1), kg/m^3
$\overline{C}_p$	intraparticle fluid phase concentration, kg/m^3
C^{sat}	initial concentration of saturated bed in elution experiments (Fig. 6), kg/m^3
D_{ax}	axial dispersion coefficient, m^2/sec
D_b	column/bed internal diameter, m
K	linear equilibrium constant, dimensionless
K'	linear equilibrium constant for a homogeneous solid ($= K + \varepsilon_p$), m^3 particle/m^3 bulk fluid
k_p	mass transfer rate constant in particle pores, sec^{-1}
k_r	reaction rate constant, sec^{-1}
k_μ	mass transfer rate constant in particle solid phase, sec^{-1}
K_r^{eq}	reaction equilibrium constant

L	TMB section length, m
L_b	bed length, m
Q	fluid flow rate according to TMB approach, m^3/sec
q_{ads}	adsorbed phase concentration (homogeneous solid), kg/m^3
$\langle \bar{q} \rangle$	intraparticle solid phase concentration, kg/kg particle
r	dimensionless isomerization reaction rate
R_p	adsorbent particle radius, m
T	temperature, K
t^*	SMB switching time, sec
U_F	fluid interstitial velocity, m/sec
U_S	solid interstitial velocity, m/sec
V_{col}	column volume, m^3
V_{el}	eluate volume, m^3
V_{ex}	extra-column volume (Eq. 1), m^3
x	space dimensionless coordinate
X	reaction conversion, %

Indexes

1, . . . ,4	TMB sections
FR	fructose
GL	glucose
Rec	recycle
F	feed
EL	eluent
X	extract
R	raffinate
eq	equilibrium

Greek Letters

ε	column void fraction, dimensionless
ε_p	adsorbent particle void fraction, dimensionless
ν	solid/fluid phase ratio $(1 - \varepsilon)/\varepsilon$, dimensionless
θ	dimensionless time coordinate
ρ_b	specific mass of immobilized enzyme in fixed-bed reactor, kg/m^3
ρ_p	adsorbent particle specific mass, kg/m^3

ACKNOWLEDGMENTS

Financial support from Capes (process 1140/96-5), Brazil, and project PRAXIS XXI/3/3.1/CEG/2644/95, Portugal, are gratefully acknowledged.

REFERENCES

1. V. P. M. S. Lima, et al., *A Cultura do Cajueiro no Nordeste do Brasil* (Banco do Nordeste do Brasil [BNB], Ed.), Fortaleza, Brazil, 1988.
2. L. A. S. Leite, *A Agroindústria do Caju no Brasil* (Empresa Brasileira de Pesquisa Agropecuária [EMBRAPA], Ed.), Fortaleza, Brazil, 1994.
3. R. L. Price, et al., *Progressive Agric. Arizona, 26*, 13 (1974).
4. A. Lopes Neto, *A Agroindústria do Caju no Nordeste do Brasil e em outros Países Grandes Produtores*, (Banco do Nordeste do Brasil [BNB], Ed.), Fortaleza, Brazil, 1981.
5. J. Johnson, in *Adsorption Science and Technology* (A. E. Rodrigues, D. Tondeur, and M. D. LeVan, Eds.), Kluwer, Dordrecht, 1989.
6. C. B. Ching and D. M. Ruthven, *AIChE Symp. Ser., 81*(242), 1 (1985b).
7. K. Hashimoto, et al., *J. Chem. Eng. Jpn., 16*(5), 400 (1983).
8. C. B. Ching, C. Ho, and D. M. Ruthven, *AIChE J., 32*(11), 1876 (1986).
9. R. M. Springfield and R. D. Hester, *Sep. Sci. Technol., 34*(6&7), 1217 (1999).
10. C. B. Ching and Z. P. Lu, *Ind. Eng. Chem. Res., 36*, 152 (1997).
11. K. Hashimoto, et al., *Biotechnol. Bioeng., 25*, 2371 (1983).
12. R. Wooley, Z. Ma, and N.-H. L. Wang, *Ind. Eng. Chem. Res., 37*, 3699 (1998).
13. M. H. C. Lopes, *Agron. Moçamb., 6*(2), 119 (1972).
14. D. C. S. Azevedo and A. E. Rodrigues, *AIChE J., 45*, 956 (1999).
15. D. C. S. Azevedo and A. E. Rodrigues, *Ind. Eng. Chem. Res., 38*, 3519 (1999).
16. L. S. Pais, J. M. Loureiro, and A. E. Rodrigues, *AIChE J., 44*, 561 (1998).
17. U. Ascher, J. Christiansen, and R. D. Russel, *ACM Trans. Math Software, 7*, 209 (1981).
18. D. M. Ruthven and C. B. Ching, *Chem. Eng. Sci., 44*, 1011 (1989).
19. F. Camacho-Rubio, E. Jurado-Alameda, P. González-Tello, and G. Luzón-González, *Can. J. Chem. Eng., 73*, 935 (1995).
20. F. A. M. Campos, *Anais Fac. Med. Univ. S. Paulo, 22*, 79 (1946).
21. P. Cen and G. T. Tsao, *Sep. Technol., 3*, 58 (1993).
22. *Ullmann's Encyclopedia of Industrial Chemistry*, 6th ed. Electronic Release, Wiley-VCH, Weinheim, 1999.

Received by editor January 21, 2000
Revision received April 2000